Nanoporous Carbons Derived from Metal-Organic Frameworks as Novel Matrices for Surface-Assisted Laser Desorption/Ionization Mass Spectrometry

Yung-Han Shih, Chien-Ping Fu, Wan-Ling Liu, Chia-Her Lin, Hsi-Ya Huang,* and Shengqian Ma**

Surface-assisted laser desorption/ionization mass spectrometry (SALDI-MS) represents a powerful tool for the analysis of biomolecules, synthetic polymers, and even small organic compounds; its performances largely depend on the type of matrix materials utilized. Here, for the first time the employment of nanoporous carbons derived from metal-organic frameworks (MOFs) as novel matrices for SALDI-MS is demonstrated. The nanoporous carbons derived from MOFs not only circumvent the shortcomings of existing matrix materials but also demonstrate much higher efficiency of laser desorption/ionization for various compounds than any other nanoporous carbons reported so far. A new perspective for the development of matrix materials for SALDI-MS application is therefore provided.

1. Introduction

Nanoporous carbons (NPCs), owing to their unique physicochemical properties such as electric conductivity, chemical stability, and thermal conductivity as well as their wide availability, have attracted great attention for diverse applications.[1] Synthesis methods including chemical vapor deposition, laser ablation, electrical arc, nanocasting, and chemical and physical activation methods have been extensively employed for the preparation of porous carbon materials.[2] Recently, a novel strategy using highly ordered crystalline metal-organic frameworks (MOFs)[3] which have excellent characteristics of high specific surface areas, tunable pore sizes, and topologies, are also used as templates or carbon sources to form porous carbon materials for applications in gas storage,[4] electrode,[5] sensor,[6] and catalysis,[7] etc. In this contribution, we demonstrate that the NPC derived from MOFs (hereafter carbonized MOFs) can serve as a new type of matrices for surface-assisted laser desorption/ionization mass spectrometry (SALDI-MS), outperforming the performances of conventional NPC-based matrices.

Matrix-assisted laser desorption/ionization (MALDI), a soft ionization technique proposed by Tanaka[8] and Karas[9] in the late 1980s, which is usually coupled with mass spectrometry (MS), has been developed into a powerful tool in the analysis of biomolecules (peptides, proteins) and synthetic polymers. Most UV-absorbing matrices used in MALDI-MS are small organic molecules (e.g., 2,5-dihydroxybenzoic acid (DHB) or α-cyano-4-hydroxycinnamic acid (HCCA)). These matrices contribute various strong signals in the low-mass region (m/z < 500 Da), which usually hinder the ability of MALDI-MS in small-mass molecule assays.[10] Furthermore, with conventional organic matrix, it is sometimes difficult to obtain homogeneous cocrystallized sample preparation and this "sweet spot" problem often leads to poor signal reproducibility between assays.

Dr. Y.-H. Shih, C.-P. Fu, Dr. W.-L. Liu, Prof. C.-H. Lin, Prof. H.-Y. Huang
Department of Chemistry
Chung Yuan Christian University
200 Chung Pei Road, Chung-Li 320, Taiwan
E-mail: chiaher@cycu.edu.tw; hyhuang@cycu.edu.tw
Prof. S. Ma
Department of Chemistry
University of South Florida
4202 East Fowler Avenue, Tampa, FL 33620, USA
E-mail: sqma@usf.edu

DOI: 10.1002/smll.201502817

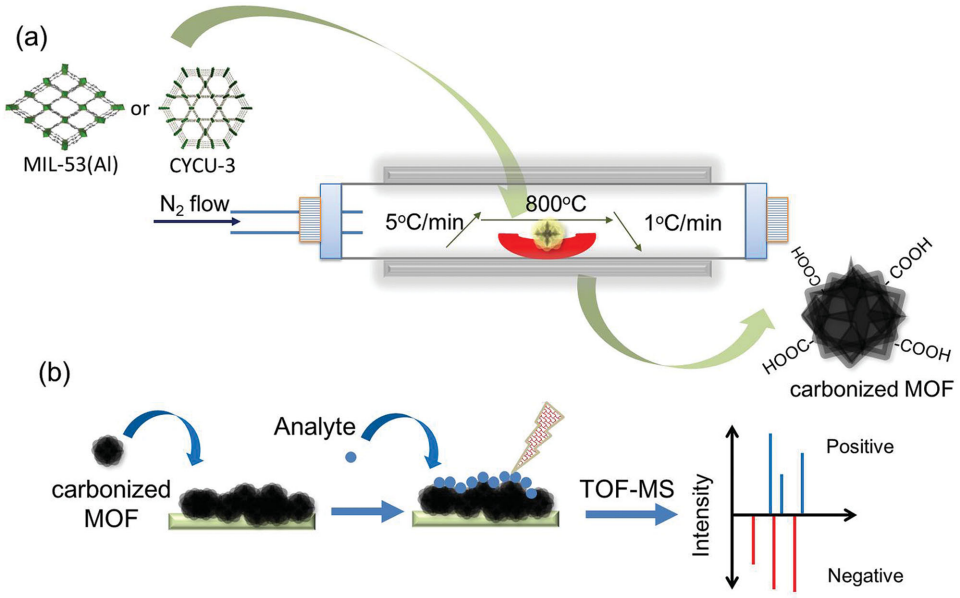

Scheme 1. a) Carbonization process of MOF; b) sample preparation process of SALDI-MS.

To overcome the aforementioned drawbacks in MALDI-MS, SALDI-MS which utilizes nanostructured surfaces as matrices in lieu of organic molecules has been developed and afforded many advantages such as very low background noise in the low-mass range, high loading capacity, high salt tolerance, excellent ability in small-molecule detection, easy sample preparation, as well as high quantitative performance, etc.[11] Among various nanostructured materials explored as matrices in SALDI-MS, carbon-based materials such as carbon nanotubes (CNTs),[12] diamond,[13] fullerene,[14] graphene,[15] graphite,[16] and activated carbons[17] have been extensively investigated and showed very efficient analyte desorption/ionization ability because they have easier functionalization,[2] higher surface area (up to 200–800 m^2 g^{-1})[2] and higher loading capacity[18] than common metal nanoparticles (such as AuNP, HgTe). In order to reduce the hydrophobicity for solubilization in aqueous solvent and proton donation, it is usually necessary to functionalize the surface of those carbon materials with —OH, —COOH or —NH_2 groups, otherwise the desorption/ionization efficiency of polar analytes would be limited.[12,15] In addition, when high laser fluency was irradiated onto NPCs such as CNTs and graphite, some carbon cluster ions can be formed thus resulting in ion suppression effect that damaged analyte's ion detection.[11b,18]

To circumvent the above shortcomings for existing carbon-based materials, herein, we propose to employ carbonized MOFs as a new type of matrices for SALDI-MS. We postulate that carbonized MOFs exhibit higher surface area, larger pore volume, and lower heat capacity than conventional carbon-based materials, as well as carry hydrophilic nature without surface modification, thus expecting to meet the high demands to serve as superior matrix for SALDI-MS. In this contribution, we report for the first time the employment of carbonized MOFs as novel matrices for SALDI-MS analysis of small molecules including polar (carbohydrates, phenolic acids and peptides) and nonpolar compounds (phthalate esters (PAEs), and polycyclic aromatic hydrocarbons (PAHs)) (**Scheme 1**). Two NPC materials, cMIL-53 and cCYCU-3, obtained from direct carbonization of MIL-53(Al) ([Al(OH)(BDC)]) (BDC = 1,4-benzenedicarboxylic acid))[19] and CYCU-3 ([Al(OH)(SDC)] (SDC = 4,4'-stilbenedicarboxylic acid)),[20] respectively (the powder X-ray diffraction (PXRD) patterns were shown in Figure S4 in the Supporting Information), via the carbonization process in Scheme 1a were used as SALDI-MS matrices in this work, meanwhile control experiments were also performed on several commercial NPC materials (CNTs, graphite, activated carbon, CMK-3 (mesoporous carbon materials with ordered structure)) as comparison.

2. Results and Discussion

2.1. Hydrophilicity Measurement

When the NPCs were mixed with ethanol or ethanol/H_2O (1:1) (5 mg per 2 mL for each), it was observed that a well-dispersed black solution was obtained for cMIL-53 and cCYCU-3 (Figure S1, Supporting Information), whereas multiwall carbon nanotube (MWCNT), single-wall carbon nanotube (SWCNT), graphite, activated carbon, and CMK-3 were immediately precipitated or precipitated gradually in ethanol and ethanol/H_2O (1:1) between 5 min and 3 h (Figure S1, Supporting Information). X-ray photoelectron spectroscopy (XPS) analysis of carbonized aluminum MOFs showed that Al 2p at 73.1 eV, Al 2s at 118.0 eV, C 1s at 283.2 eV, and O 1s at 531.2 eV indicate that Al_2O_3 still exist in the carbonaceous materials (**Figure 1**a). For more information about the features of carbonized MOFs, high-resolution XPS of deconvolution C 1s peak illustrates an obvious characteristics of C=C at 283.8 eV and carbonyl group[21] such as C—O, C=O, and O—C=O at 284.3, 287.7, and 292.5 eV, respectively, for cMIL-53 (Figure 1b) and cCYCU-3 (Figure 1c), which is similar to the

small NANO MICRO

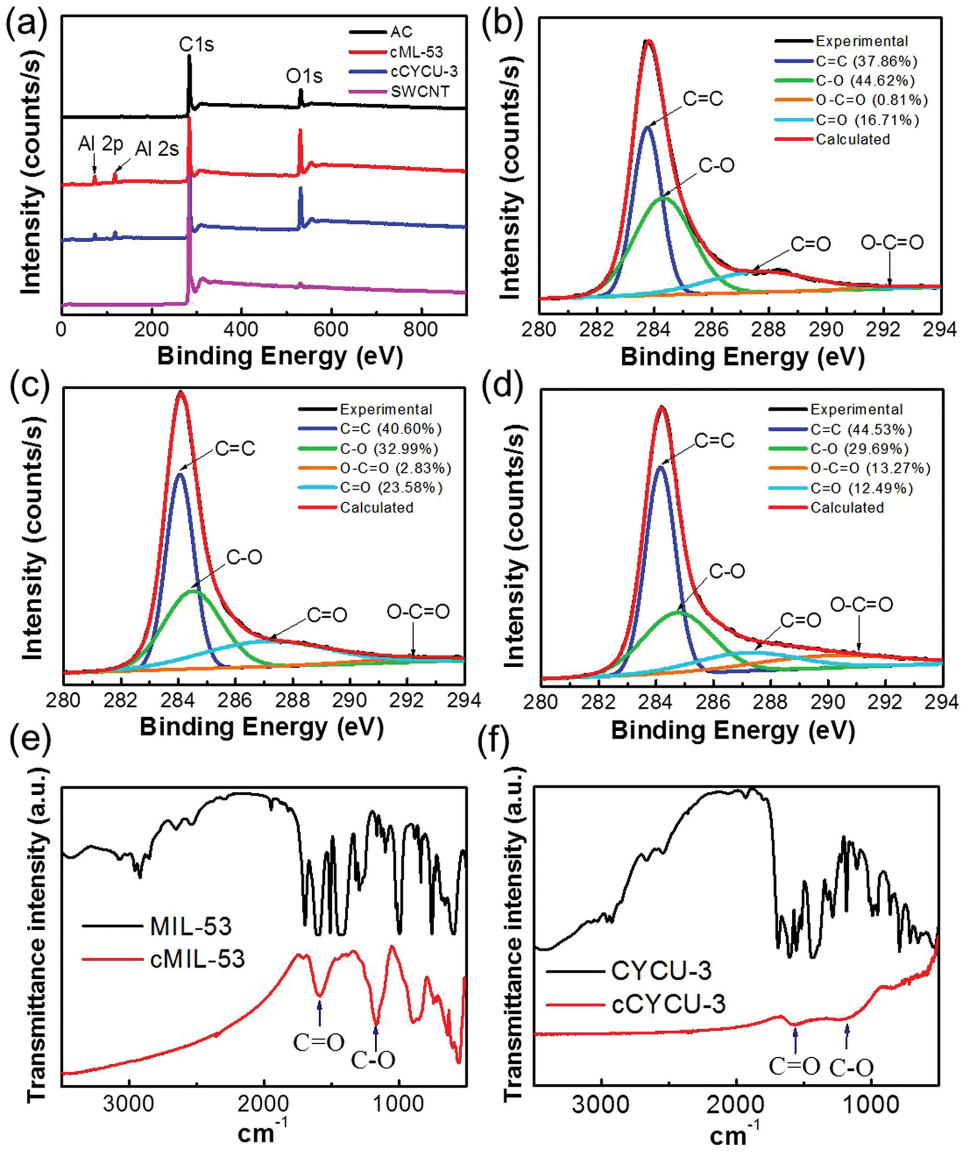

Figure 1. a) Wide-range XPS spectra of NPCs. Curve fit of the C1s peak of b) cMIL-53, c) cCYCU-3, and d) activated carbon (AC). FTIR spectra of e) cMIL-53 and f) cCYCU-3.

activated carbon (Figure 1d). Since the carbonization used in Scheme 1a had undergone in N_2 gas atmosphere, the high ratios of C—O, C=O, and O—C=O signals relative to total carbon (C 1s) signals (62.14 and 59.4% for cMIL-53 and cCYCU-3, respectively) should be ascribed to the contribution of carboxylic acid residues from MOF's organic linkers. Fourier transform infrared spectroscopy (FTIR) spectra of cMIL-53 and cCYCU-3 (Figure 1e,f) revealed the absorption bands at 1588 and 1165 cm^{-1} associated with the characteristic C=O and C—O stretching vibrations of carboxylic group, suggesting the existence of hydrophilic —COOH moieties in carbonized MOFs; in contrast, no hydrophilic groups are existent in other NPCs as also indicated by FTIR studies (Figure S2, Supporting Information), except for activated carbon.

The hydrophilicity of the carbonized MOFs was determined by water vapor adsorption at room temperature. As shown in **Figure 2**a, very minimum water adsorption at low relative pressure (such as P/P_0 = 0.1–0.3) was observed in activated carbon, while significant uptake arose under higher relative pressure, implying that the activated carbon belongs to Type V isotherm (the most common in porous carbon).[22] In contrast, 8 wt% of water adsorption at P/P_0 = 0.3 was obtained in cMIL-53 with an obvious shift in the inflection point at lower relative pressure suggesting a Type IV isotherm.[22] Obviously, it indicates that cMIL-53 is more hydrophilic than activated carbon.[23] Furthermore, due to the apparent hydrogen bonding between water molecule and COOH-functionalized MOF's surface, water can immediately be adsorbed onto the hydrophilic cMIL-53 even at low pressure (P/P_0 = 0.1).[24] In addition, the remaining of Al_2O_3 in cMIL-53, which is a Lewis acid, also enhances the water vapor adsorption[25] with 15 wt% total water uptake higher than activated carbon (9 wt%) despite their comparable amount of COOH group to each other. This also accounts for the high dispersibility of cMIL-53 in polar aqueous solution as observed in Figure S1 (Supporting Information).

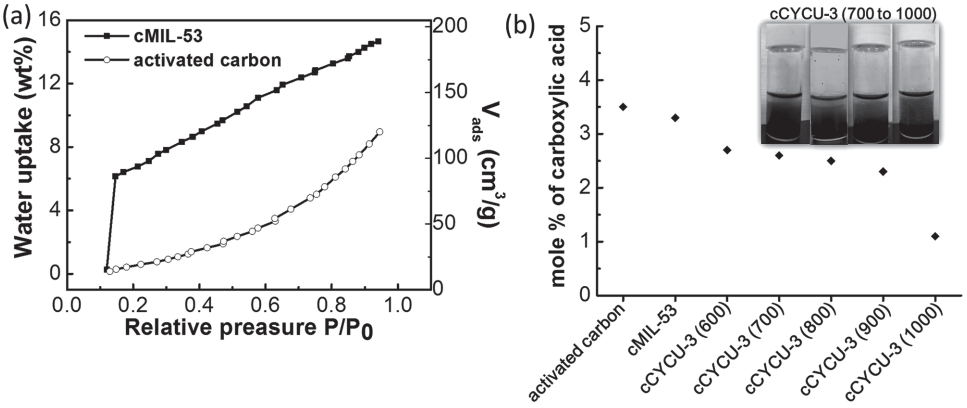

Figure 2. a) Water vapor adsorption of cMIL-53 and activated carbon measured at room temperature. b) The mole percentages of carboxylic acid groups in NPCs (inset: the dispersibility of cCYCU-3 obtained at different pyrolysis temperature in ethanol/water (1:1, v/v)).

To quantify the carboxylic groups present in the carbonized MOFs, forward acid–base titration with $NaHCO_3$ aqueous solution was conducted (see the Experimental Section). By calculation,[26] the mole percentages of COOH in activated carbon, cMIL-53, and cCYCU-3 were 3.5%, 3.3%, and 2.7%, respectively (Figure 2b), suggesting that a residual carboxylic acid from BDC or SDC linkers was retained in the carbonized MOFs, which was consistent with the obtained results in XPS and FTIR spectra (Figure 1). Further investigations on the variance of carboxylic acid residues using different pyrolysis temperature were evaluated for cCYCU-3 (600–1000 °C, referred as cCYCU-3 (600–1000)). As shown in Figure 2b, the mole percentage of COOH in cCYCU-3 was highly dependent on the carbonization temperature (2.6% and 1.1% for cCYCU-600 and cCYCU-1000, respectively), and the cCYCU-3 obtained at higher carbonization temperature has lower carboxylic acid residues, resulting to a poor dispersibility in polar solvent (Figure 2b, inset). Since higher carbonization temperature enhances the pyrolysis of MOF's organic linkers, different COOH-functionalized NPC material can be formed via simple controlled temperature to carbonize the MOFs. Collating all of the above results (dispersibility test in polar solvent, measurements using XPS, FTIR, and acid–base titration), therefore concludes that the proposed simple carbonization step (Scheme 1a) could generate a hydrophilic carbonized MOFs with better dispersibility in polar solvents (e.g., ethanol or ethanol/H_2O commonly used for SALDI-MS matrix preparation) as compared with other NPCs of CNTs, activated carbon, and CMK-3.

2.2. Characterization of Carbonized MOFs

Raman spectra of cMIL-53 as well as cCYCU-3 exhibit D- and G-band signals at 1345 and 1588 cm^{-1}, respectively, which are consistent with common NPCs such as MWCNT, SWCNT, and graphite (**Figure 3**a,b, and Figure S3, Supporting Information). Therefore, it can be inferred that both cMIL-53 and cCYCU-3 are constituted by disordered carbon structures of the C=C (sp^2) bonding. In general, the higher intensity ratio of D and G bands (I_D/I_G) represents the higher disordered structure of carbon materials,[6,27] and the ratio of I_D/I_G is 1.13 and 1.18 for cMIL-53 and cCYCU-3, respectively (between SWCNT (0.17) and MWCNT (1.68)) indicate the highly disordered/defective nature of porous carbonized MOFs. Furthermore, the PXRD patterns of cMIL-53 and cCYCU-3 revealed broad peaks at 2θ = 13°(001), 25°(002), and 44°(101) corresponding to those of graphene and graphite,[4] suggesting the coexistence of both structures in carbonized MOFs (Figure 3c,d; Figure S4, Supporting Information).

Scanning electron microscopy (SEM) and transmission electron microscopy (TEM) images (**Figure 4**) revealed very similar surface structures and shapes between the pristine and carbonized MOFs, illustrating that the original morphology of these Al-based MOFs was well retained after carbonization. Also, XPS, SEM-EDS (energy dispersive X-ray spectroscopy), as well as TEM-EDS analysis showed the retained Al_2O_3 (4.63% and 2.19% for cMIL-53 and cCYCU-3, respectively) in carbonized MOFs after pyrolysis (Figure 1a; Figure S39 and Table S4, Supporting Information). Moreover, SEM images clearly show the highly defective surface accompanied with large cracks and voids, while high-resolution TEM (HRTEM) images indicate a randomly oriented graphenic/graphic layer inside the cMIL-53 and cCYCU-3 (Figure 4d,h), which are also consistent with previous literatures,[4b–d,5b] as further confirmed by the above PXRD and Raman studies.

The N_2 sorption isotherms collected at 77 K reveal the BET surface areas of 1145 and 365 $m^2\ g^{-1}$ for cMIL-53 and cCYCU-3, respectively, and pore sizes predominantly distributed around 1.4 nm for cMIL-53 while a broad pore size distribution from 2.2 to 17 nm was observed for cCYCU-3 (**Figure 5**) due to the seriously defect and the shrinkage effect of some specific MOFs for carbonization process.[4d,5c,7c] Combining with HRTEM results (Figure 4d,h), both micropores and mesopores are confirmed in the carbonized MOFs.

2.3. Adsorption Mode

To investigate the adsorption behavior when using cMIL-53 as absorbent, a small molecule, methylene blue (MB, 10 mg L^{-1}), was used as the model compound.[28] The time-dependent

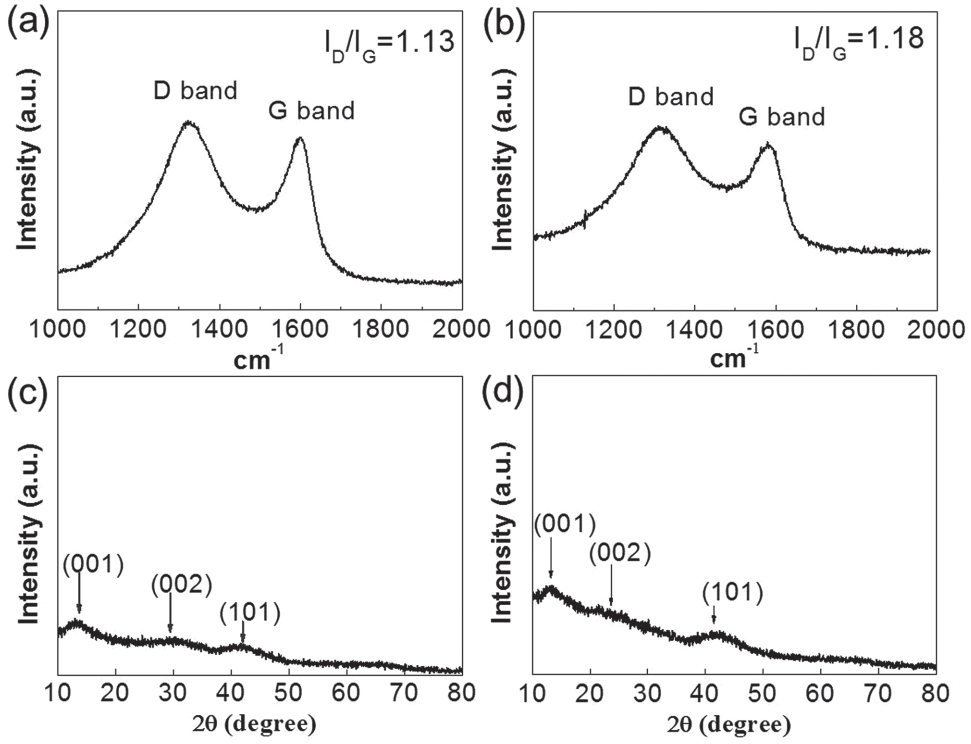

Figure 3. Raman spectra of a) cMIL-53 and b) cCYCU-3; PXRD pattern spectra of c) cMIL-53 and d) cCYCU-3.

adsorption of MB on cMIL-53 (**Figure 6**a; Figure S7, Supporting Information) shows an 83.1% adsorption capability in 5 min as well as a maximum loading capacity (2.5 mg MB g^{-1} cMIL-53) at 4 h. Moreover, the trend of enhanced adsorption capacity of cMIL-53 with increasing MB concentration (Figure 6b) also indicates the favorable adsorption of small molecules obtained on carbonized MOF when at high concentration.[28]

2.4. SALDI-MS Analysis of Small Molecules

Considering that the high hydrophilicity and high surface area could improve the "sweet spot" problem as well as enhance the loading capacity in SALDI-MS analysis, we decided to employ cMIL-53 as matrices for SALDI-MS analysis for polar and nonpolar compounds via the process illustrated in Scheme 1b. When the pristine MIL-53(Al) (noncarbonized MOF)

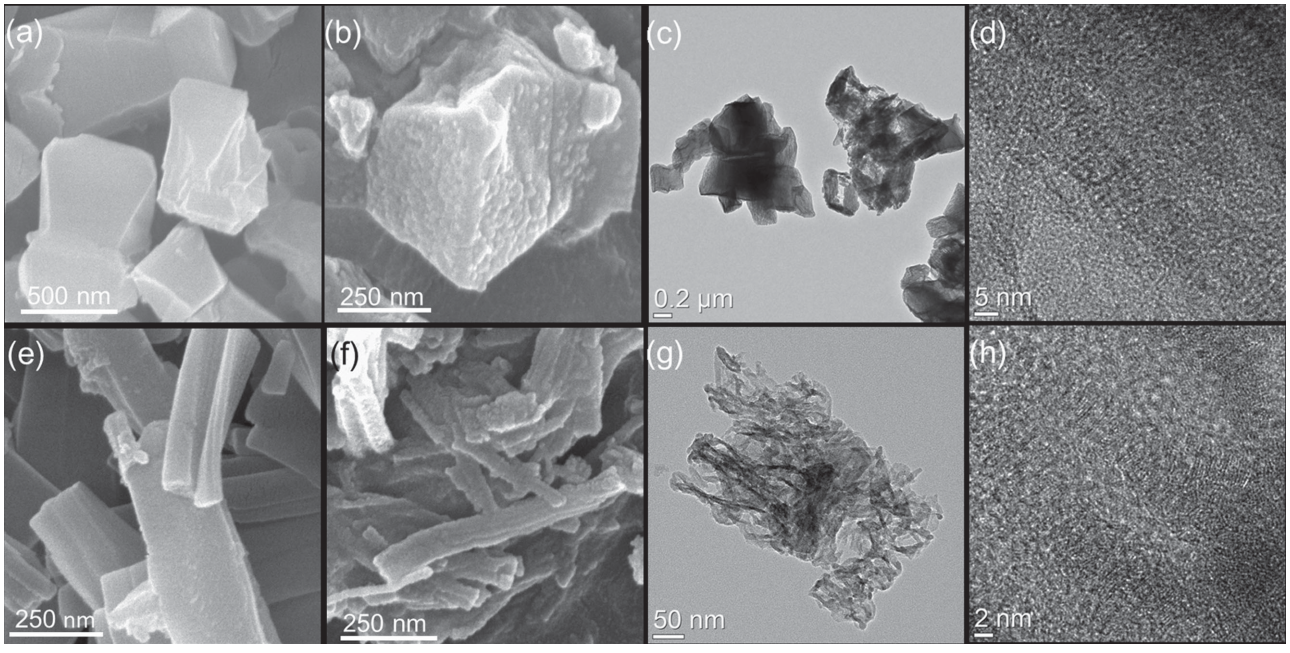

Figure 4. SEM images of a) MIL-53(Al), b) cMIL-53, e) CYCU-3, and f) cCYCU-3. TEM images of c,d) cMIL-53 and g,h) cCYCU-3.

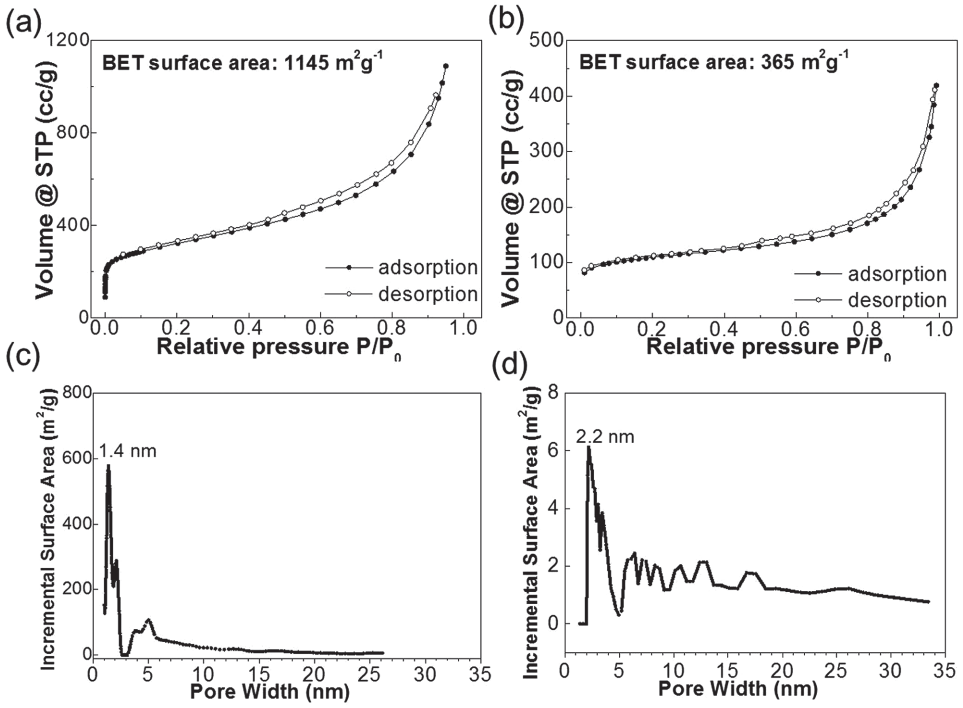

Figure 5. N_2 gas adsorption/desorption isotherm of a) cMIL-53 and b) cCYCU-3. Pore size distribution of c) cMIL-53 and d) cCYCU-3.

is utilized as matrix, none of the carbohydrates can be detected (**Figure 7**a; Figure S10, Supporting Information); in contrast, strong ion signals accompanied with clean mass spectra in the low-mass range were obtained using cMIL-53 as matrix. The carbohydrates were detected as $[M+Na]^+$, $[M+K]^+$, or $[M-C_2H_4O_2+Na]^+$ (Figure 7b; Figure S13, Supporting Information), similar to what reported in previous literatures when using HCCA or DHB as matrix (Figures S11 and S12, Supporting Information).[29]

As suggested from previous report, if the carbonized Al-based MOF was further treated with hydrofluoric acid (HF) to remove the residue of Al component (here referred as HF-cMIL-53), the surface area and pore volume could be greatly increased.[5c,6] However, for comparison in our case, when cMIL-53 or HF-cMIL-53 was used as matrix, the desorption/ionization efficiency of SALDI-MS analysis of neutral carbohydrates was similar to each other (Figure S40, Supporting Information). We postulated that the COOH functionality and the UV-absorbing ability of cMIL-53 and HF-cMIL-53 were almost identical (Figures S2 and S6, Supporting Information). In order to find out the role of Al_2O_3 (Lewis acid) for SALDI-MS analyses, basic amino acids (histidine, lysine, and arginine) were used as Lewis base compounds.[30] As shown in **Figure 8**a, when cMIL-53 was used as a matrix, significant mass signals were detected in proton or alkali metal adduct while none or very low intensities for HF-cMIL-53 (Figure 8b). The results indicate that the presence of Al_2O_3 in cMIL-53 enhances the ionization ability of basic amino acids through Lewis-acid/base interaction (electron acceptor/donor) and hydrophilicity-induced interaction between the cMIL-53 and polar compounds. Hence, to increase the functionality (COOH and Lewis acid (Al_2O_3)) and prevent the cost of time (four days needed for HF washing) and generate more waste, we preferred cMIL-53 as a matrix for the following experiments. Moreover, cMIL-53 matrix is also applicable to analyze the amino acids with high salt concentration (775×10^{-3} m NaCl) that indicating its high salt tolerance (Figure 8c,d, and Figure S41, Supporting Information).

Tables S1 and S2 (Supporting Information) summarize the quantitative performances of the carbohydrates using cMIL-53 as matrix, which shows the relative standard deviations (RSDs) of signal-to-noise ratio (S/N) around 7%–12% and limit of detections (LODs) ranging from 137 to 241 nM. These results are better

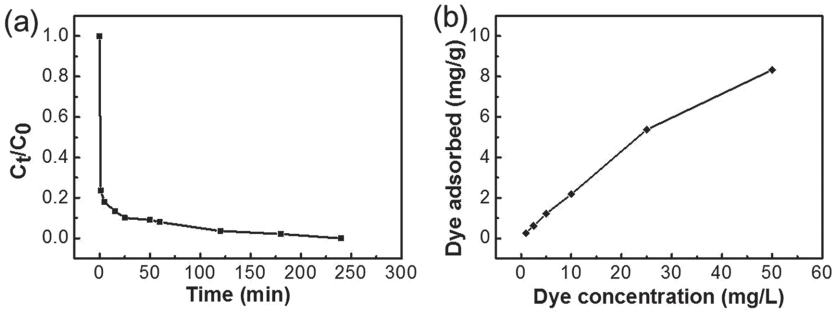

Figure 6. a) Molar ratio of methylene blue (10 mg L^{-1}) adsorbed on cMIL-53 at different adsorption time. b) Standard adsorption curve of methylene blue on cMIL-53. Each data were calculated from the UV–vis absorbance of MB (λ_{max} = 660 nm). C_0 is defined as the UV–vis absorbance of MB solution at initial time (0 min); while C_t is the UV–vis absorbance of MB solution at specific time.

than or comparable with those reported previously in the literature (Table S1, Supporting Information). SALDI-MS analysis of other small molecules with different polarity was also performed using cMIL-53 as matrix with high reproducibility of S/N and no interferences in mass spectra (Table S3, Supporting Information). To illustrate the advantages of carbonized MOFs as SALDI-MS matrices, another carbonized MOF, cCYCU-3, was evaluated for its desorption/ionization ability for all the analytes tested in this work. Similar to cMIL-53, cCYCU-3 resulted in clean mass spectra in all mass regions for either polar or nonpolar molecule detections (Figures S15 and S16, Supporting Information). Our previous report on the evaluation of MOFs as SALDI-MS matrices indicated unstable signals as well as serious matrix interferences obtained from tunnel-type MOFs (e.g., CYCU-3(Al)) as matrices and nonpolar PAHs compounds as analytes.[31] However, the above results suggest that the carbonization process shown in Scheme 1 avoids the release of organic linkers (SDC) from the CYCU-3 during laser irradiation. Similar results were

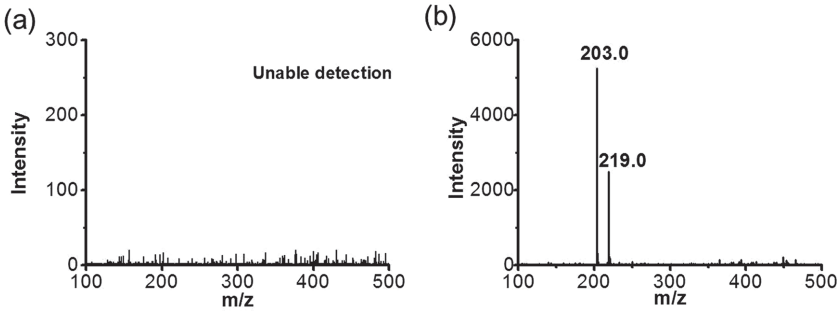

Figure 7. SALDI-MS spectra of glucose (*m/z* 203.0, $[M+Na]^+$; *m/z* 219.0, $[M+K]^+$) using a) MIL-53(Al) and b) cMIL-53 as matrix. Laser intensity: 35%.

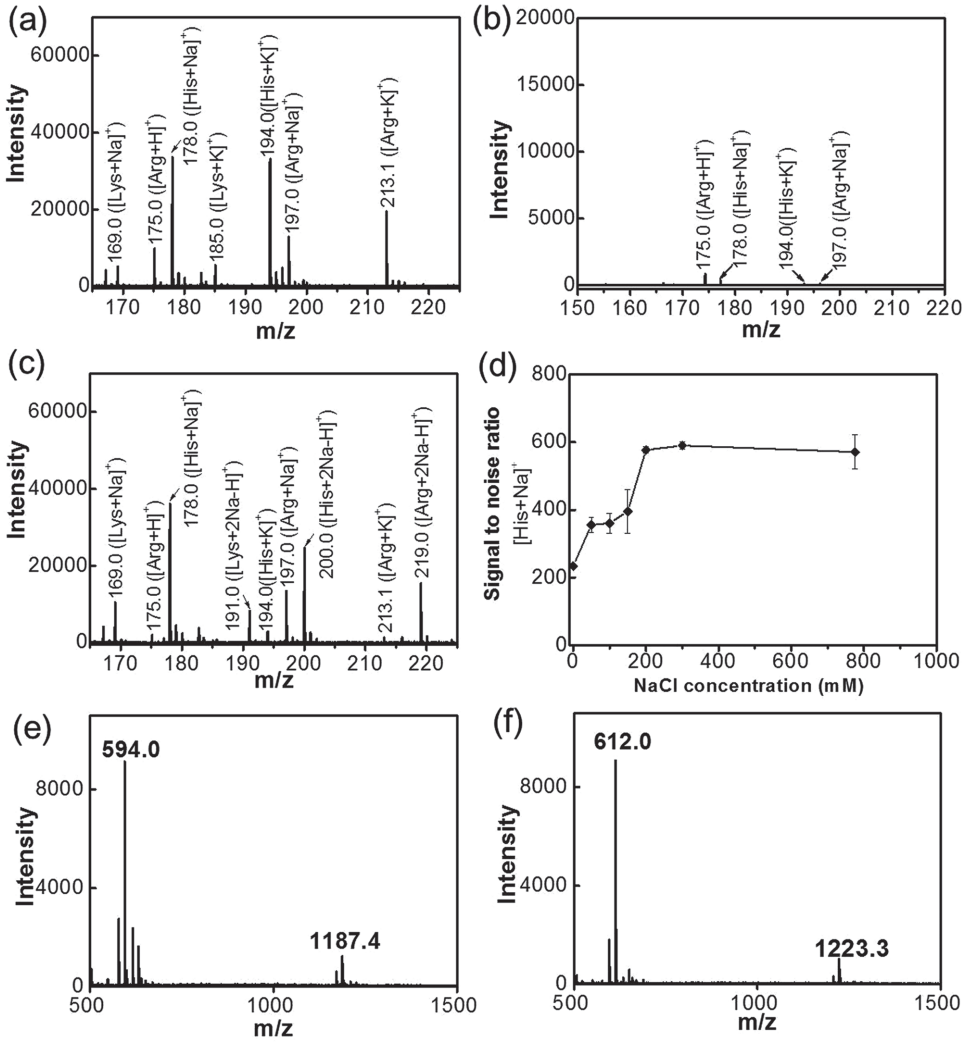

Figure 8. SALDI-MS analysis of four basic amino acids containing a,b) 0×10^{-3} m NaCl and c) 775×10^{-3} m NaCl by using a,c) cMIL-53 and b) HF-cMIL-53 matrix. d) The effect of salt concentration on signal-to-noise ratio of $[His+Na]^+$. (*m/z* 169.0, $[Lys+Na]^+$; *m/z* 191.0, $[Lys+2Na-H]^+$; *m/z* 185.0, $[Lys+K]^+$; *m/z* 178.0, $[His+Na]^+$; *m/z* 200.0, $[His+2Na-H]^+$; *m/z* 194.0, $[His+K]^+$; *m/z* 200.1, $[His+2Na-H]^+$; *m/z* 175.0, $[Arg+H]^+$; *m/z* 197.0, $[Arg+Na]^+$; *m/z* 219.0, $[Arg+2Na-H]^+$; *m/z* 213.0, $[Arg+K]^+$). SALDI-MS spectra of peptides e) Leu-Enk (*m/z* 594.0 $[M+K]^+$, *m/z* 1187.4 $[2M+K]^+$) and f) Met-Enk (*m/z* 612.0 $[M+K]^+$, *m/z* 1223.3 $[2M+K]^+$), with cMIL-53 matrix.

also obtained using carbonized MOF-5[32] and ZIF-8[4e] (Figures S36–S38, Supporting Information).

To demonstrate the superiority of carbonized MOFs as novel matrices, different NPCs including MWCNT, SWCNT, graphite, activated carbon, and CMK-3 were also examined. A poor signal reproducibility was observed for most compounds (Figures S28–S32 and Table S2, Supporting Information). This is due to the fact that CNTs, graphite, activated carbon, and CMK-3 are prone to aggregate when they are dispersed in the commonly used solvents for matrix preparation (Figure S1, Supporting Information), thus leading to possible "sweet-spot" phenomenon. In addition, in contrast to most CNTs and graphite, which often need additional surface modification to improve their suspension in aqueous and organic solvents as well as to enhance their adsorption capability of analytes, carbonized MOFs when used as matrix have better dispersibility and stronger interactions with polar solutes (Figures S1, S8, and S9, Supporting Information), thereby capable of providing comparable or better S/N for all test molecules.

It has been known that, due to the strong UV absorption,[11b] low heat capacity,[11a,18] and high surface area,[2] CNTs are regarded as the best carbon-based matrices for efficient desorption/ionization of small molecules. In comparison, an even higher surface area (compare their surface areas here, Figure S5, Supporting Information) but a lower specific heat capacity (C_p = 2.40, 0.67, and 0.13 J g^{-1} K^{-1} at 225 °C for MWCNT, SWCNT, and cMIL-53, respectively, **Figure 9**) are observed for cMIL-53. This means, when compared to both CNTs materials, a higher temperature change can be produced when the laser irradiated the cMIL-53 surface (generally above 200 or 250 °C needed in most cases),[31] thus resulting in a higher energy transfer to the analytes, thereby leading to a more efficient desorption/ionization via thermally driven process.[11]

In terms of graphite, despite its low specific heat capacity (C_p = 0.7 J g^{-1} K^{-1} at 25°C)[18b] when used as matrix, some molecules (for example, four of eight PAEs and one of three PAHs) cannot be detected even at very weak ion signals (Figures S22, S23, and S28–S32, Supporting Information). We deduce that when compared to CNTs and carbonized MOFs, graphite has the lowest UV absorption ability (Figure S6, Supporting Information), thus laser-induced internal energy transferred from graphite matrix to analytes is still inadequate to cause the desorption and ionization of small-molecule analytes.[18]

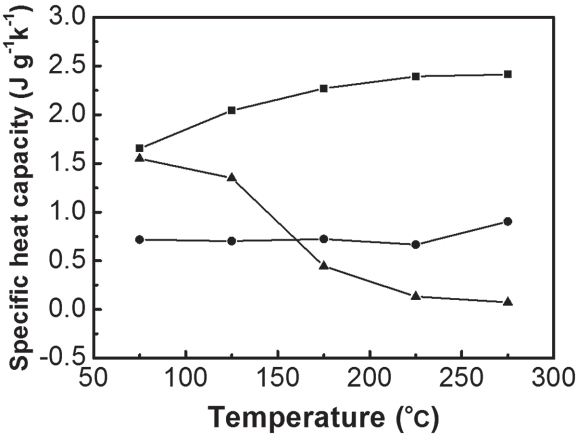

Figure 9. Specific heat capacity (C_p) of NPCs at different temperatures. MWCNT (■); SWCNT (●); cMIL-53 (▲).

Regarding to larger molecule mass peptides (Leu-enkephalin (Leu-Enk) and Met-enkephalin (Met-Enk)), no or very weak signals are detected when CNTs, graphite, and activated carbon serve as matrices (Figure S32, Supporting Information), possibly due to the formation of some carbon cluster ions (highlighted with 12 m/z units apart in Figure S35, Supporting Information) which in turn cause a significant ion suppression effect to lower peptide ion production.[11b] In contrast, when cMIL-53 and cCYCU-3 (RSD of S/N has the lowest value showed in Table S2 in the Supporting Information) are employed as matrices, their intact potassium adduct ions ($[Leu\text{-}Enk+K]^+$, $[Met\text{-}Enk+K]^+$) as well as $[2Leu\text{-}Enk+K]^+$ and $[2Met\text{-}Enk+K]^+$ peptide dimer ions appear[33] as shown in Figure 8e,f and Figure S16d,e (see in the Supporting Information). These results indicate that the employment of carbonized MOFs as matrices also can provide a soft ionization/desorption process to minimize the damage of large molecules such as peptides under laser irradiation.

To quantitatively evaluate the performance of cMIL-53 as matrix, one of the PAEs, diethylhexyl phthalate (DEHP), which is the major pollutant among PAEs because of its widespread use and occurrence in the environment,[34] is subsequently employed as the model analyte. As shown in Figure S33 (Supporting Information), the calibration curve constructed with the signal intensity ratio of $[DEHP+Na]^+$ to $[DIDP+Na]^+$ (internal standard) shows a good linearity (R^2 > 0.994) in the concentration range of 1–200 ppm. Because of its large surface area (1145 m^2 g^{-1}), cMIL-53 can play the role of solid-phase extraction adsorbent to trap trace level DEHP (1 μg mL^{-1}), thus enabling the enhancement in detection sensitivity of SALDI-MS analysis (LOD from 23.9 (± 3.5) ppb to 4.0 (± 0.2) ppb (Figure S34, Supporting Information)), which is in accordance with United States Environmental Protection Agency (U.S. EPA) regulation for DEHP in drinking water (< 6 ppb).[35] These results highlight the potential of cMIL-53 as both matrix and adsorbent in SALDI-MS analysis for important biomolecules and ubiquitous environmental pollutants.

3. Conclusion

We present a new approach in preparing NPCs with uniform pore structures, COOH pore surfaces, and carrying Lewis acid component (Al_2O_3) (in contrast to the hydrophobic pore surfaces of the conventional carbon materials) via controlled carbonization of MOFs. The resulted NPCs have been employed for the first time as a new type of matrices for SALDI-MS analyses of various polar and nonpolar compounds, outperforming the existing matrix materials. Due to their low heat capacity and high UV absorptivity of the carbonized MOFs, they demonstrate much higher efficiency desorption/ionization of polar and nonpolar small-molecule analytes without any matrix interferences in the low-mass

region compared with the pristine MOFs and other NPCs. For instance, the RSD% of S/N for carbohydrates was around 7%–12%, 9%–80%, 60%–130%, 60%–150%, 40%–220%, and 7%–80% for cMIL-53, MWCNT, SWCNT, graphite, activated carbon, and CMK-3, respectively. This work thereby not only advances MOF-derived carbon materials in the applications of analytical fields but also illustrates a new route in the preparation of different COOH-functionalized NPC materials with controlled temperature to carbonize MOFs, which opens a new door for developing functional hydrophilic NPCs in the future.

4. Experimental Section

Synthesis of MOFs: MIL-53(Al), [Al(OH)(BDC)], was synthesized according to the procedure reported in the literature.[19] CYCU-3, [Al(OH)(SDC)], was synthesized and activated according to published procedures.[20]

Synthesis of Carbonized MOFs: cMIL-53 and cCYCU-3 were synthesized and activated according to published procedures.[6] MOF powders of 200 mg were placed into a ceramic boat then transferred in the furnace. The furnace was then heated under a nitrogen gas flow from room temperature to 600–1000 °C at a rate of 5 °C min^{-1}. After the temperature reached the established settings, it was maintained for 5 h and then cooled to room temperature at a rate of 1 °C min^{-1}. For HF washing step, the obtained black powders were then stirred in 20% HF. After 24 h, the black precipitates were collected by centrifugation. In order to completely remove the aluminum components, the washing step was repeated four times. Afterward, the HF-washed precipitates were further cleaned with D.I. water and then dried under vacuum conditions overnight at 40 °C.

Acid–Base Titration: The procedure of forward titration was based on the previous report[26] with slight modification to determine the amount of carboxylic acid in NPCs. Generally, three (3) mg of dried NPC was suspended in excess 0.05 n $NaHCO_3$ (2 mL) and magnetically stirred at room temperature for 3 d. After centrifugation (supernatant was set aside), the NPC precipitate was washed with 5 mL D.I. water for three times to remove the unreacted $NaHCO_3$, then, combined with the supernatant; and subsequently added into 0.05 m HCl solution (2 mL) and boiled for 5 min to remove the present CO_2. After cooling to room temperature, the solution was titrated with 0.05 m $NaOH_{(aq)}$ until pH 7.0 (Mettler Toledo, Switzerland). The total titrated volumes for activated carbon, cMIL-53, and cCYCU (600–1000) were 175, 132, 120, 115, 110, 105, and 50 µL, respectively.

Methylene Blue Adsorption: For time-dependent adsorption, two (2) mg of dried cMIL-53 was added into 10 mg L^{-1} of MB solution (ethanol/H_2O (1:1, v/v)). After gentle vortex at specific time (1, 5, 15, 25, 50, 60, 120, 180, and 240 min), the adsorbed MB solution obtained by centrifugation was analyzed using UV–vis spectrometry (Shimadzu, Japan). The effect of dye concentration on the MB amount adsorbed on cMIL-53 was operated as the follows: 2 mg of dried cMIL-53 was added into MB solution at different concentration (1, 2.5, 5, 10, 25, and 50 mg L^{-1}), and then vortex for 60 min. After centrifugation, the solution was examined by UV–vis spectrometry.

Sample Preparation for MALDI- or SALDI-MS: The HCCA matrix (10 mg) was dissolved in 0.1% trifluoroacetic acid (TFA) in 1 mL D.I. water/ACN (5/95, v/v). The DHB matrix (10 mg) was dissolved in 0.1% TFA in 1 mL D.I. water/ACN (3:7, v/v). The carbonized MOFs or MOFs (1 mg) were dispersed separately in 2 mL solution of ethanol and sonicated for 3 min each. The CNTs (5–12 nm diameter, >1 µm length) were obtained from Golden Innovation Business Co. Ltd (New Taipei city, Taiwan). Graphite flake (1–10 µm, >99% purity) was purchased from Alfa Aesar (Ward hill, USA). Activated carbon (100–400 mesh) was obtained from Aldrich (Steinheim, Germany). Commercial ordered mesoporous carbon, CMK-3 (surface area: ≈1000 m^2 g^{-1}; pore diameter: 5.57 nm, total pore volume: 1.35 cm^3 g^{-1}), was purchased from ACS Material. One (1) mg of each CNT, graphite and activated carbon were dispersed separately in 2 mL D.I. water/ethanol (1:1, v/v). Matrix first method was used for SALDI-MS sample preparation. Briefly, 1 µL of the suspension (HCCA, DHB, carbonized MOFs, or other NPCs) was pipetted onto the stainless steel target plate. After drying, 1 µL solution of analytes was pipetted onto the same position of the stainless steel target plate and left in the air for 2–3 min for solvent evaporation. It was left in the air at room temperature for 5–10 min to form a thin layer, and then ready for further analysis by MALDI- or SALDI-MS.

Mass Spectrometry: Ultraflextreme MALDI-MS (Bruker Daltonics) equipped with a 355 nm Nd:YAG-laser at 66.7 Hz was used to detect carbohydrates, PAEs, PAHs, and peptides. For amino acid analysis, the dada were acquired on Autoflex speed MALDI-MS (Bruker Daltonics) equipped with a 355 nm Nd:YAG-laser at 100 Hz. All the analysis was performed under reflectron positive-ion mode, while phenolic acids were under reflectron negative-ion mode. The available accelerating voltage existed in the range from +25kV to −25kV. In order to obtain a good S/N, the laser power (20%–40%) was adjusted to slightly above the threshold.

Supporting Information

Supporting Information is available from the Wiley Online Library or from the author.

Acknowledgements

Y.-H.S. and C.-P.F. contributed equally to this work. The authors are grateful for financial support by grants MOST 103–2632M-033-001-MY3 and MOST 104–2113M-033–003-MY3 from the Ministry of Science and Technology of Taiwan. The authors also thank Prof. Chien-Chieh Hu for the XPS measurement.

[1] a) S. L. Candelaria, Y. Shao, W. Zhou, X. Li, J. Xiao, J.-G. Zhang, Y. Wang, J. Liu, J. Li, G. Cao, *Nano Energy* **2012**, *1*, 195; b) L. Hu, D. S. Hecht, G. Grüner, *Chem. Rev.* **2010**, *110*, 5790; c) S. Xin, Y.-G. Guo, L.-J. Wan, *Acc. Chem. Res.* **2012**, *45*, 1759; d) S. Zhao, H. Yin, L. Du, G. Yin, Z. Tang, S. Liu, *J. Mater. Chem. A* **2014**, *2*, 3719; e) S. Zhao, Y. Li, H. Yin, Z. Liu, E. Luan, F. Zhao, Z. Tang, S. Liu, *Sci. Adv.* **2015**, *1*, e1500372.

[2] a) C. Liang, Z. Li, S. Dai, *Angew. Chem., Int. Ed.* **2008**, *47*, 3696; *Angew. Chem.* **2011**, *120*, 3754; b) C. Liang, Z. Li, S. Dai, *Angew.*

Chem. **2011**, *120*, 3754; c) J. Lee, J. Kim, T. Hyeon, *Adv. Mater.* **2006**, *18*, 2073; d) B. Hu, K. Wang, L. Wu, S.-H. Yu, M. Antonietti, M.-M. Titirici, *Adv. Mater.* **2010**, *22*, 813.

[3] a) H.-C. Zhou, J. R. Long, O. M. Yaghi, *Chem. Rev.* **2012**, *112*, 673; b) H.-C. Zhou, S. Kitagawa, *Chem. Soc. Rev.* **2014**, *43*, 5415; c) W.-Y. Gao, M. Chrzanowski, S. Ma, *Chem. Soc. Rev.* **2014**, *43*, 5841; d) Q.-L. Zhu, Q. Xu, *Chem. Soc. Rev.* **2014**, *43*, 5468; e) W.-Y. Gao, M. Chrzanowski, S. Ma, *Chem. Soc. Rev.* **2014**, *43*, 5841; f) Y. He, B. Li, M. O'Keeffe, B. Chen, *Chem. Soc. Rev.* **2014**, *43*, 5618; g) L. Lux, K. Williams, S. Ma, *CrystEngComm* **2015**, *17*, 10; h) J.-K. Su, Q. Xu, *Energy Environ. Sci.* **2014**, *7*, 2071; i) L. He, Y. Liu, J. Liu, Y. Xiong, J. Zheng, Y. Liu, Z. Tang, *Angew. Chem. Int. Ed.* **2013**, *52*, 3741; j) L. He, Y. Liu, J. Liu, Y. Xiong, J. Zheng, Y. Liu, Z. Tang, *Angew. Chem.* **2013**, *125*, 3829; k) Y. Liu, Z. Tang, *Adv. Mater.* **2013**, *25*, 5819.

[4] a) B. Liu, H. Shioyama, T. Akita, Q. Xu, *J. Am. Chem. Soc.* **2008**, *130*, 5390; b) H.-L. Jiang, B. Liu, Y.-Q. Lan, K. Kuratani, T. Akita, H. Shioyama, F. Zong, Q. Xu, *J. Am. Chem. Soc.* **2011**, *133*, 11854; c) S. Lim, K. Suh, Y. Kim, M. Yoon, H. Park, D. N. Dybtsev, K. Kim, *Chem. Comm.* **2012**, *48*, 7447; d) H. J. Lee, W. Cho, E. Lim, M. Oh, *Chem. Commun.* **2014**, *50*, 5476; e) G. Srinivas, V. Krungleviciute, Z.-X. Guo, T. Yildirim, *Energy Environ. Sci.* **2014**, *7*, 335.

[5] a) B. Liu, H. Shioyama, H. Jiang, X. Zhang, Q. Xu, *Carbon* **2010**, *48*, 456; b) P. Su, L. Jiang, J. Zhao, J. Yan, C. Li, Q. Yang, *Chem. Commun.* **2012**, *48*, 8769; c) W. Chaikittisilp, K. Ariga, Y. Yamauchi, *J. Mater. Chem. A* **2013**, *1*, 14; d) F. Zou, X. Hu, Z. Li, L. Qie, C. Hu, R. Zeng, Y. Jiang, Y. Huang, *Adv. Mater.* **2014**, *26*, 6622; e) T. Y. Ma, S. Dai, M. Jaroniec, S. H. Qiao, *J. Am. Chem. Soc.* **2014**, *136*, 13925.

[6] M. Hu, J. Reboul, S. Furukawa, N. L. Torad, Q. Ji, P. Srinivasu, K. Ariga, S. Kitagawa, Y. Yamauchi, *J. Am. Chem. Soc.* **2012**, *134*, 2864.

[7] a) S. Ma, G. A. Goenaga, A. V. Call, D.-J. Liu, *Chem. Eur. J.* **2011**, *17*, 2063; b) W. Chaikittisilp, N. L. Torad, C. Li, M. Imura, N. Suzuki, S. Ishihara, K. Ariga, Y. Yamauchi, *Chem. Eur. J.* **2014**, *20*, 4217; c) Z. Dong, X. Le, Y. Liu, C. Dong, J. Ma, *J. Mater. Chem. A* **2014**, *2*, 18775; d) A. Aijaz, N. Fujiwara, Q. Xu, *J. Am. Chem. Soc.* **2014**, *136*, 6790; e) S. Zhao, H. Yin, L. Du, L. He, K. Zhao, L. Chang, G. Yin, H. Zhao, S. Liu, Z. Tang, *ACS Nano* **2014**, *8*, 12660.

[8] K. Tanaka, H. Waki, Y. Ido, S. Akita, Y. Yoshida, T. Yoshida, *Rapid Commun. Mass Spectrom.* **1988**, *2*, 151.

[9] M. Karas, D. Bachmann, F. Hillenkamp, *Anal. Chem.* **1985**, *57*, 2935.

[10] J. J. A. van Kampen, P. C. Burgers, R. de Groot, R. A. Gruters, T. M. Luider, *Mass Spectrom. Rev.* **2011**, *30*, 101.

[11] a) C.-K. Chiang, W.-T. Chen, H.-T. Chang, *Chem. Soc. Rev.* **2011**, *40*, 1269; b) R. Arakawa, H. Kawasaki, *Anal. Sci.* **2010**, *26*, 1229.

[12] a) C. Shi, J. Meng, C. Deng, *J. Mater. Chem.* **2012**, *22*, 20778; b) Y.-K. Kim, H.-K. Na, S.-J. Kwack, S.-R. Ryoo, Y. Lee, S. Hong, S. Hong, Y. Jeong, D.-H. Min, *ACS Nano* **2011**, *5*, 4550; c) X.-S. Li, J.-H. Wu, L.-D. Xu, Q. Zhao, Y.-B. Luo, B.-F. Yuan, Y.-Q. Feng, *Chem. Commun.* **2011**, *47*, 9816; d) J. Meng, C. Shi, C. Deng, *Chem. Commun.* **2011**, *47*, 11017.

[13] Y. Coffinier, S. Szunerits, H. Drobecq, O. Melnyk, R. Boukherroub, *Nanoscale* **2012**, *4*, 231.

[14] W. E. Wallace, *Chem. Commun.* **2007**, *43*, 4525.

[15] a) Q. Liu, M. Cheng, G. Jiang, *Chem.-Eur. J.* **2013**, *19*, 5561; b) Y.-K. Kim, D.-H. Min, *Langmuir* **2012**, *28*, 4453.

[16] S. Zumbühl, R. Knochenmuss, S. Wülfert, F. Dubois, M. J. Dale, R. Zenobi, *Anal. Chem.* **1998**, *70*, 707.

[17] a) T. T. Hoang, Y. Chen, S. W. May, R. F. Browner, *Anal. Chem.* **2004**, *76*, 2062; b) M. Han, J. Sunner, *J. Am. Soc. Mass Spectrom.* **2000**, *11*, 644.

[18] a) K. P. Law, J. R. Larkin, *Anal. Bioanal. Chem.* **2011**, *399*, 2597; b) H.-W. Tang, K.-M. Ng, W. Lu, C.-M. Che, *Anal. Chem.* **2009**, *81*, 4720.

[19] T. Loiseau, C. Serre, C. Huguenard, G. Fink, F. Taulelle, M. Henry, T. Bataille, G. Férey, *Chem.-Eur. J.* **2004**, *10*, 1373.

[20] S.-H. Lo, C.-H. Chien, Y.-L. Lai, C.-C. Yang, J. J. Lee, D. S. Raja, C.-H. Lin, *J. Mater. Chem. A* **2013**, *1*, 324.

[21] a) T. Sun, Z. Zhang, J. Xiao, C. Chen, F. Xiao, S. Wang, Y. Liu, *Sci. Rep.* **2013**, *3*, 2527; b) O. Jankovský, P. Šimek, D. Sedmidubský, S. Huber, M. Pumera, Z. Sofer, *RSC Adv.* **2014**, *4*, 7418; c) Y. Cheng, H. Zhang, V. Varanasi, J. Liu, *Sci. Rep.* **2013**, *3*, 3195.

[22] S. Lagorsse, M. C. Campo, F. D. Magalhães, A. Mendes, *Carbon* **2005**, *43*, 2769.

[23] N. C. Burtch, H. Jasuja, K. S. Walton, *Chem. Rev.* **2014**, *114*, 10575.

[24] H. Ito, T. Iiyama, S. Ozeki, *J. Phys. Chem. C* **2015**, *119*, 4118.

[25] H. A. Al-Abadleh, V. H. Grassian, *Langmuir* **2003**, *19*, 341.

[26] a) N. Amini, M. Shariatgorji, G. Thorsén, *J. Am. Soc. Mass Spectrom.* **2009**, *20*, 1207; b) H. Hu, P. Bhowmik, B. Zhao, M. A. Hamon, M. E. Itkis, R. C. Haddon, *Chem. Phys. Lett.* **2001**, *345*, 25.

[27] L. Radhakrishnan, J. Reboul, S. Furukawa, P. Srinivasu, S. Kitagawa, Y. Yamauchi, *Chem. Mater.* **2011**, *23*, 1225.

[28] A. Banerjee, R. Gokhale, S. Bhatnagar, J. Jog, M. Bhardwaj, B. Lefez, B. Hannoyer, S. Ogale, *J. Mater. Chem.* **2012**, *22*, 19694.

[29] D. J. Harvey, *Int. J. Mass Spectrom.* **2003**, *226*, 1.

[30] M. M. Stone, A. H. Franz, C. B. Lebrilla, *J. Am. Soc. Mass. Spectrom.* **2002**, *13*, 964.

[31] Y.-H. Shih, C.-H. Chien, B. Singco, C.-L. Hsu, C.-H. Lin, H.-Y. Huang, *Chem. Commun.* **2013**, *49*, 4929.

[32] J. A. Thompson, C. R. Blad, N. A. Brunelli, M. E. Lydon, R. P. Lively, C. W. Jones, S. Nair, *Chem. Mater.* **2012**, *24*, 1930.

[33] K. Strupat, *Methods Enzymol.* **2005**, *405*, 1.

[34] C. A. Staples, D. R. Peterson, T. F. Parkerton, W. J. Adams, *Chemosphere* **1997**, *35*, 667.

[35] United States Environmental Protection Agency (U.S. EPA), National Primary Drinking Water Regulations **2009**, EPA 816-F-09-004 (http://water.epa.gov/drink/contaminants/basicinformation/di_2-ethylhexyl_phthalate.cfm).

Received: September 17, 2015
Revised: February 1, 2016
Published online: February 23, 2016